Acta Crystallographica Section D
Biological Crystallography
ISSN 0907-4449

Structure of a king cobra phospholipase A_2 determined from a hemihedrally twinned crystal

Sujuan Xu,[a] Lichuan Gu,[a] Qiuyan Wang,[b] Yuyan Shu,[b] Shiying Song[a] and Zhengjiong Lin[a]*

[a]National Laboratory of Biomacromolecules, Institute of Biophysics, Chinese Academy of Sciences, Beijing 100101, People's Republic of China, and [b]Institute of Snake Venoms, Guangxi Medical University, Nanning 530021, People's Republic of China

Correspondence e-mail: lin@sun5.ibp.ac.cn

Received 7 April 2003
Accepted 30 June 2003

PDB Reference:
OH $APLA_2$-II, 1m8t, r1m8tsf.

An acidic PLA_2 (OH $APLA_2$-II) from the venom of *Ophiophagus hannah* (king cobra) shows greater phospholipase A_2 activity and weaker cardiotoxic and myotoxic activity than a homologous acidic PLA_2 from the same venom. The crystal of the enzyme belongs to space group $P6_3$. The crystals are invariably hemihedrally twinned, exhibiting perfect 622 Laue symmetry. The structure was determined by molecular replacement and refined using a hemihedral twinning program at 2.1 Å resolution. The final model has reasonable stereochemistry and a crystallographic R factor of 19.5% ($R_{\rm free}$ = 21.5%). The structure reveals the molecular arrangement and the mode of twinning. There are six independent molecules in the asymmetric unit. Owing to the presence of a non-crystallographic twofold parallel to the hemihedral twinning twofold, the molecular packing in the twinned crystal is extremely similar to that in an untwinned crystal for four of the molecules. This unique molecular arrangement may be related to the difficulty in recognizing the twinning. The structure was compared with the previously determined structure of a homologous acidic PLA_2 from the same source. The comparison shows structural changes that might be implicated in the increased catalytic activity and weakened toxicity.

1. Introduction

Phospholipase A_2 (PLA_2; EC 3.1.1.4) is one of the most important enzymes for the metabolism of lipids. It catalyzes the hydrolysis of the fatty-acid ester at the *sn*-2 position of phospholipids. Calcium cations are essential both for substrate binding and for catalysis (de Haas *et al.*, 1971; Verheij *et al.*, 1980). In addition to being a catalyst for the hydrolysis of phospholipids, most PLA_2s from snake venom also possess a wide variety of pharmacological activities, such as neurotoxic, myotoxic, haemolytic, anticoagulant and antiplatelet activities (Kini, 1997). The structural basis of the myotoxicity and cardiotoxicity is still largely unknown.

Ophiophagus hannah (king cobra) is the largest venomous snake in the world and has a distribution range limited to South China and Southeast Asia. Several PLA_2 enzymes have been isolated and characterized from its venom (Tan & Saifuddin, 1990; Chiou *et al.*, 1995; Huang *et al.*, 1997). Two acidic PLA_2s were isolated from the venom of a king cobra captured in the Guangxi province of China and were designated OH $APLA_2$ (pI = 5.5, MW = 13 719 Da; Wang, Zhuang *et al.*, 2001) and OH $APLA_2$-II (pI = 4.0, MW = 13 174 Da; Wang, 2001). They belong to different subgroups, 1B and 1A,

respectively (Davidson & Dennis, 1990). Sequence comparison (Wang, Shu *et al.*, 2001) showed that OH $APLA_2$-II (subgroup 1A) does not possess the 'pancreatic loop' (a five-amino-acid insertion at residues 62–66; Arni & Ward, 1996) which is present in OH $APLA_2$ (subgroup1B) and that the two subgroups have a shared identity of 75%. Despite the high sequence homology, they have significant differences in their biological activity. OH-$APLA_2$ causes myotoxicity and cardiotoxicity in laboratory animals, while these were scarcely observed on injection of OH $APLA_2$-II (Wang, 2001). In addition, the phospholipase A_2 activity of OH $APLA_2$-II is much greater than that of OH $APLA_2$ (Wang, 2001). The crystal structure of OH $APLA_2$ has been determined to 2.6 Å resolution in our laboratory (Zhang *et al.*, 2002). In this paper, we report the structure determination of OH $APLA_2$-II at 2.1 Å resolution and describe the structural features that may be responsible for the increased enzyme activity and weakened toxicity by comparing the structures of OH $APLA_2$-II and OH $APLA_2$.

Twinning may be an obstacle to the determination of a macromolecular crystal structure in some special space groups (Yeates, 1997). In the case of merohedral twinning, the crystal contains several consistently disoriented regions (twin domains) that are related by a symmetry operation (twinning operation). The diffraction patterns of the twin domains are exactly superimposed, so the observed intensity of every reflection is a sum of the true intensities from all twin domains, assuming that interference effects can be ignored. Thus, the intensity distribution instead of the diffraction patterns should be used to recognize merohedral twinning. Several programs have been established to test the merohedral twinning of protein crystals based on intensity distribution (Yeates, 1997). Hemihedral twinning is a special case of merohedral twinning in which there are only two twin domains. When the volumes of the two domains are equal, the twinning is said to be perfect. Perfectly hemihedral twinning results in a higher order symmetry in the diffraction pattern than the true symmetry of the crystal space group. Molecular replacement has allowed the determination of several protein structures from this type of hemihedrally twinned crystal (*e.g.* Redinbo & Yeates, 1993; Gomis-Rüth *et al.*, 1995; Breyer *et al.*, 1999; Ramadan *et al.*, 2002). This paper reports the structure determination of OH $APLA_2$-II by molecular replacement from a perfectly hemihedrally twinned crystal, the twinning of which cannot be recognized by the normal intensity-distribution testing method.

2. Materials and methods

2.1. Crystallization and data collection

The enzyme used for crystallization was extracted from the venom of *O. hannah* (collected from Gugangxi Province, China) according to a procedure outlined previously (Wang, 2001). The enzyme showed significant catalytic activity. Crystals were grown at 291 K by the hanging-drop method with 10 mg ml^{-1} protein, 3.4 *M* 1,6-hexanediol, 0.2 *M* magnesium chloride and 0.1 *M* Tris–HCl buffer pH 8.5 in 8 µl drops equilibrated against 0.5 ml well solution consisting of 0.1 *M* Tris–HCl buffer pH 8.5 and 6 *M* 1,6-hexanediol. Crystals with dimensions of 0.6 × 0.6 × 0.3 mm were found in the drops after one month. The detailed crystallization procedure and preliminary X-ray characterization of the crystal have been reported elsewhere (Xu *et al.*, 2002).

Table 1
Data-collection results.

Values in parentheses are for the highest solution shell (2.17–2.10 Å).

Space group	$P6_3$
Unit-cell parameters (Å, °)	$a = b = 98.06$, $c = 132.39$, $\gamma = 120$
Resolution range (Å)	17.0–2.1
R_{merge} (%)	7.8 (38.3)
Completeness of data (%)	99.9 (98.8)
Average $I/\sigma(I)$	38.1 (7.4)
Total No. of observations	1527037
Total No. of unique reflections	41966

Data were collected on a MAR 345 image-plate detector (MAR Research; λ = 1.54178 Å) using a perfectly hemihedrally twinned crystal at a temperature of 100 K with a crystal-to-detector distance of 185 mm. The total rotation range was from 0 to 320° with an oscillation angle of 1° and an exposure time of 60 s per frame. The data were scaled and merged using the *HKL* suite (Otwinowski & Minor, 1997). The data processed in space group $P6_3$ had an R_{merge} of 7.8%, whereas the data processed in space group $P6_322$ had an R_{merge} of 8.8% without an obvious increase in rejected reflections. Thus, the probable space group seems to be either $P6_3$ or $P6_322$. The unit-cell parameters are $a = b = 98.06$, $c = 132.39$ Å. The self-rotation function from the data merged in space group $P6_3$ gave a peak with a height of 99.6% of the origin peak, indicating a twofold axis perpendicular to crystallographic 6_3 screw axis and the crystallographic *b* axis. This result seems to support space group $P6_322$. However, the space group was verified to be $P6_3$ after molecular replacement and crystallographic refinement (see the following sections). The data-collection results are summarized in Table 1.

2.2. Molecular replacement

The structure was solved by the molecular-replacement method using the *MOLREP* program (Vagin & Teplyakov, 1997). The structure of PLA_2 from the venom of *Naja atra* was selected as a search model (PDB code 1poa, without water molecules and Ca atoms; Scott *et al.*, 1990), as it belongs to same subgroup as OH $APLA_2$-II and has 69% sequence identity. The residues that differed between the two enzymes were treated as alanines. The molecular-replacement study was first carried out in space group $P6_322$. Three molecules (*A*, *B* and *C*) were found in the asymmetric unit. The initial model, oriented and positioned according to the molecular-replacement solution, was examined on a Silicon Graphics O2 workstation using the program *TURBO-FRODO* (Jones,

Table 2
Molecular replacement.

α, β, γ are Eulerian angles; θ, φ, χ are polar angles; x, y, z are fractional Cartesian coordinates; Rf is the peak height of the rotation function; R is the R factor; Corr is the correlation coefficient.

(a) Cross-rotation function.

Peak	α (°)	β (°)	γ (°)	θ (°)	ψ (°)	χ (°)	Rf	Rf/σ
1	53.15	73.47	51.85	43.25	90.65	121.60	1426	7.79
2	6.49	105.10	231.07	123.87	157.71	145.95	1415	7.73
3	44.98	72.92	50.52	44.95	87.23	114.53	1213	6.63
4	15.13	107.10	230.48	121.83	162.33	142.45	1206	6.59
5	5.47	64.96	315.52	117.68	114.97	74.66	630	3.44

(b) Translation function.

Solution No.	Peak	α (°)	β (°)	γ (°)	x	y	z	R	Corr
1	1	53.15	73.47	51.85	0.522	0.123	0.000	0.575	0.209
2	1	53.15	73.47	51.85	0.856	0.790	0.545	0.563	0.311
3	2	6.49	105.10	−128.93	0.524	0.399	0.258	0.534	0.353
4	2	6.49	105.10	−128.93	0.857	0.066	0.802	0.530	0.391
5	3	44.98	72.92	50.52	0.167	0.472	0.000	0.515	0.425
6	4	15.13	107.10	−129.52	0.165	0.695	0.257	0.489	0.460

Table 3
Refinement results.

Twinned R factor (%)	19.5
Twinned $R_{\rm free}$ factor (%)	21.5
Detwinned R factor (%)	19.3
Detwinned $R_{\rm free}$ factor (%)	21.2
Resolution range (Å)	17.0–2.1
No. of reflections	41938
Model	
No. of protein atoms	5473
No. of calcium ions	6
No. of 1,6-hexanediol molecules	10
No. of water molecules	855
R.m.s. deviations from ideality	
Bond distances (Å)	0.009
Bond angles (°)	1.46
Dihedral angles (°)	23.47
Improper angles (°)	0.87

1978). It was found that molecule B seriously overlapped with its crystallographically symmetrical molecule, resulting in poor corresponding $2F_o - F_c$ electron density, and that there were no obvious $2F_o - F_c$ or $F_o - F_c$ electron-density peaks at the site expected for a calcium ion. Better results were obtained from the molecular-replacement study in space group $P6_3$. In this case, six PLA_2 molecules (A, B, C, D, E and F) were found in each asymmetric unit (see Table 2 for details). Subsequent rigid-body refinement using *CNS* (Brünger *et al.*, 1998) gave an R factor of 44.3% (using 17–3 Å resolution data). The crystal packing was found to be reasonable. A strong $2F_o - F_c$ and $F_o - F_c$ electron-density peak was found in every molecule at the site expected for a calcium ion. Thus, the molecular-replacement study confirmed the space group to be $P6_3$.

2.3. Structure refinement

The refinement was carried out using *CNS* with 5% of the data reserved for calculation of the free R factor (Brünger, 1992). A total of 41 938 reflections in the resolution range 17–2.1 Å were used in the refinement. The main chains and side chains of the molecules were adjusted stepwise according to the $2F_o - F_c$ and $F_o - F_c$ electron-density maps. Some side chains that were changed to alanines in the initial search model during molecular replacement were determined according to the electron-density maps and amino-acid sequence reported previously (Wang, Shu *et al.*, 2001). After atomic positions were refined, the R value fell to 37.5%. A simulated-annealing refinement was carried out by decreasing the temperature in 30 K steps from an initial value of 3600 K, which reduced the R value to 34.8%. The main chains and side chains of the molecules were stepwise adjusted and atomic positions were again refined. The R value then fell to 33.2% with an $R_{\rm free}$ value of 36.0%. Further adjustment and refinement did not reduce the R or $R_{\rm free}$ values further. Meanwhile, two molecules (B and F) had poor $2F_o - F_c$ electron density, although the other four molecules (A, C, D and E) had continuous and well defined $2F_o - F_c$ electron density.

The diffraction data shows perfect Laue symmetry, $P6_322$, indicating the presence of a perfectly hemihedral twinned crystal symmetry, although the twinning testing program (from http://www.doe-mbi.ucla.edu/Services/Twinning/) did not recognize the twinning. Hemihedral twinning refinement programs from *CNS* were then used in the following model rebuilding and refinement. After the first round of refinement, the twinned R value and twinned $R_{\rm free}$ value decreased to 27.2 and 26.7%, respectively, and the electron-density map of molecules B and F improved significantly. The main chains and side chains of the molecules were adjusted and calcium ions and 1,6-hexanediol molecules were identified based on their electron-density maps and environments. Water molecules were found first automatically using the *CNS* program and were then confirmed by their electron-density maps and environments. After several steps of atomic position and B-factor refinement, the final twinned R value fell to 19.5%, with a twinned $R_{\rm free}$ value of 21.5%, and the detwinned R fell to 19.2%, with a detwinned $R_{\rm free}$ value of 21.3%.

The final model had good stereochemical quality, with the r.m.s. deviations from the ideal value being 0.009 Å for bond lengths and 1.46° for bond angles. Calculations using the program *PROCHECK* (Laskowski *et al.*, 1993) indicated that all non-glycine and non-proline residues in the asymmetric unit were located in most favored regions (511 residues) or additional allowed regions (103 residues). The Ramachandran plot of the main-chain torsion angles (Ramachandran & Sasisekharan, 1968) showed that 83.2% of the residues were in the most favored regions, with none of the residues in the disallowed regions. The refinement results are listed in Table 3.

3. Results and discussion

3.1. Crystal packing and twinning

The structure of OH $APLA_2$-II reveals that each of six independent molecules in the asymmetric unit forms a trimer-like structure together with its crystallographic threefold-related molecules (Fig. 1) and that the six trimers are related by three non-crystallographic twofold axes, forming three trimer pairs: *A* and *C*, *D* and *E*, and *B* and *F*. All the three non-crystallographic twofold axes are approximately parallel to the *a** axis. Of these, the two non-crystallographic twofold axes of the *AC* and *DE* pairs are located at the same *z* value, while the location of the non-crystallographic twofold axis of the *BF* pair deviates from that of the other two pairs by about 5 Å along the crystallographic *c* axis. For true symmetry of point group 6, the additional symmetry induced by perfectly hemihedral twinning is a twofold parallel to the crystallographic *a** (or *a*, *b* and *b**) axis (Yeates, 1997). Thus, in this case, the perfectly hemihedral twinning twofold is parallel to the non-crystallographic twofold. Supposing that the twinning twofold coincides with the non-crystallographic twofold of the *AC* pair (or *DE* pair), the molecular packing in the twinned crystal is extremely similar to that in an untwinned crystal for molecules *A*, *C*, *D* and *E* (Figs. 2*a* and 2*b*). This may be why refinement of these molecules using the untwinned-crystal program worked well. On the other hand, the situation is quite different for the remaining two molecules, where the twinning twofold does not coincide with the non-crystallographic twofold (deviation from 5 Å along the *c* axis), leading to the overlap of the *BF* pair with its crystallographic symmetry-related pair. Thus, the abnormal behavior for molecules *B* and *F* in the refinement when an untwinned crystal is under consideration can be explained by ignoring the twinning.

Figure 1
Trimer structure viewed down the crystallographic *c* axis and drawn as a ribbon. Some hydrophobic side chains are shown. Note: the programs *MOLSCRIPT* (Kraulis, 1991) and *Raster3D* (Merritt & Bacon, 1997) were used for drawing this figure.

As reported previously (Chandra *et al.*, 1999; Breyer *et al.*, 1999) clues that diffraction data may be from a perfectly

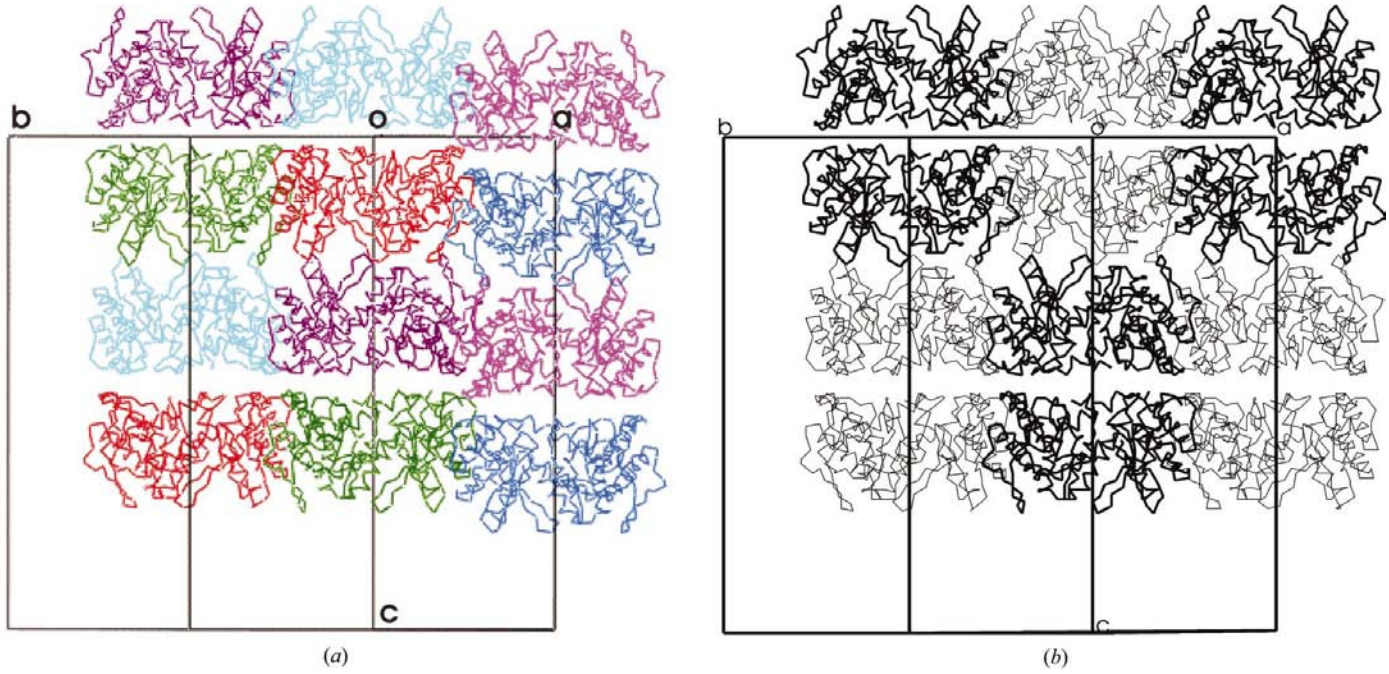

Figure 2
A packing diagram of an untwinned crystal viewed down the crystallographic *a** axis; the protein molecules are drawn as a C^{α} trace. (*a*) All molecules, *A* (green), *B* (deep blue), *C* (deep purple), *D* (red), *E* (blue) and *F* (purple), are shown. (*b*) Four molecules, *A* (thick), *C* (thick), *D* (thin) and *E* (thin), are shown. The non-crystallographic twofold of trimers *AC*, *DE* and *BF* are parallel to the *a** axis, but only those of *AC* and *DE* are located at $z = 0$. The molecular packing in a hemihedrally twinned crystal should be similar to that in this untwinned crystal for molecules *A*, *C*, *D* and *E*.

twinned crystal include: (i) the unit cell not being large enough to contain the known molecules found during molecular replacement under the apparent space-group symmetry and (ii) the intensity distribution not following Wilson statistics (Wilson, 1949). For the latter test, several related expressions can be computed. One is the value of $\langle I^2\rangle/\langle I\rangle^2$, which is expected to be 1.5 for (acentric) twinned data and 2.0 for (acentric) untwinned data. The test must be performed on normalized data or in thin shells (Yeates, 1997). In the case of OH APLA$_2$-II, the asymmetric unit can accommodate all the molecules found during molecular replacement and the value of $\langle I^2\rangle/\langle I\rangle^2$ is about 2.3. Both account for the failure to recognize twinning in the early stages of the structure determination. The unique property of the molecular arrangement, *i.e.* the similarity in molecular packing between the twinned and untwinned crystal for the four molecules (*A*, *C*, *D* and *E*), may be one of the reasons that the number of molecular-replacement solutions is not doubled as in a usual twinning case and the $\langle I^2\rangle/\langle I\rangle^2$ value is higher than expected.

3.2. Overall structure

The final model consists of 5473 non-H protein atoms from six crystallographically independent molecules, six calcium ions, ten 1,6-hexanediol molecules and 855 water molecules. These atoms occupy 65% of the unit-cell volume. The $2F_o - F_c$ electron-density map is continuous and well defined for both the backbone and the side chains, with the exception of a very small number of polar side chains on the molecule surface. Fig. 3 shows segment 15–20 with its corresponding electron density. In this experiment, no calcium ions were added to the crystallization solutions; however, a strong electron-density peak at the expected calcium-ion position around the calcium-binding loop indicated the presence of calcium ions (Figs. 4*a*, 4*b*). Similar cases have been reported previously (Wang *et al.*, 1996). As mentioned above, every molecule and its two crystallographic threefold-axis related molecules seemed to form a trimer with 6.7% of the monomer surface area buried. A light-scattering experiment showed the enzyme to exist in a monomeric state in solution (data not shown). Thus, the trimer-like structure observed in the crystal state may not be of significance.

The six molecules in an asymmetric unit have similar overall structures. The obvious differences are confined to segment 14–20, the reverse turn of the β-wing and the C-terminus ridge, as well as two surface loops: 85–91 and 57–60. Fig. 5 shows six molecules after least-squares superposition of C^{α} atoms. Segment 14–20 together with the C-terminus ridge involve a great number of residues at the interface-recognition site (IRS; Dijkstra *et al.*, 1981). The flexibility of these residues was suggested to be a common feature of PLA$_2$ and to be required by the 'allosteric activity' during the enzyme–oil/water interface interaction (Gu *et al.*, 2002). In group II PLA$_2$s, the β-wing (75–85) was found to adopt a variety of orientations in relation to the main body of the molecule. In group I PLA$_2$s a disulfide bond (11–77) connects the β-wing to the body, restricting the orientation of the wing. Nevertheless, this work shows that the reverse turn (78–81) of the β-wing in group I PLA$_2$s could be mobile. The conformation of a calcium-binding loop bound to a calcium ion is known to be conservative, with the calcium ion being coordinated to seven (or six) oxygen ligands: three from backbone carbonyls of the highly conserved residues Tyr28, Gly30, Gly32, two from the carboxyl group of Asp49 and two (or one) from water molecules (Arni & Ward, 1996). In molecules *A*, *C*, *D*, *E* and *F*, the loops have conformations similar to those in the normal seven-coordination cases. Unexpectedly, the loop in molecule *B* has a significantly different conformation. In this conformation, only one O atom from the carboxyl group of Asp49 coordinates to the calcium ion. The equivalent atoms in the calcium-binding loop in molecule *B* and the other molecules have the largest deviation, at more than 2 Å. The structure of the loop in molecule *B* is reliable, as is shown by its well defined $2F_o - F_c$ electron-density maps (Fig. 4*b*). There is no significant packing difference between *B* and the others and there are very few hydrogen-bonding or hydrophobic interactions involved in the

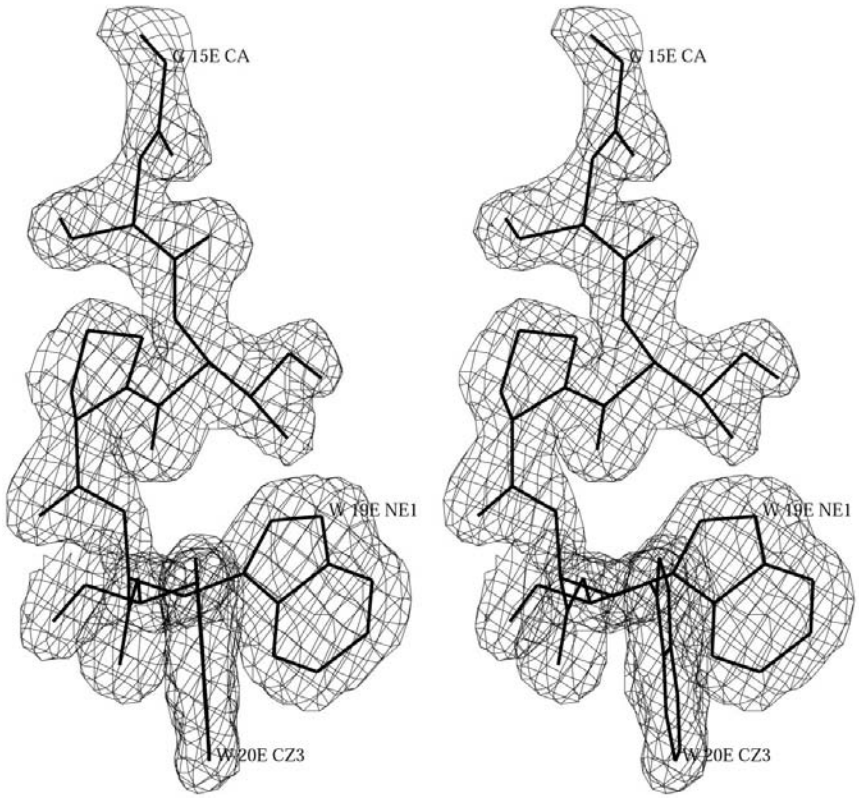

Figure 3
$2Fo - F_c$ electron-density map contoured at 1.5σ of segment 15–20 in molecule *E*.

calcium-binding loop. Also, it is unlikely that this arises from lower occupancy of the calcium ion, as the calcium ion binding to molecule *B* has an electron-density peak height similar to those of other calcium ions. At the moment, the reason why molecule *B* has a unique calcium-binding loop conformation which is not related to the crystal packing and calcium occupancy is unclear.

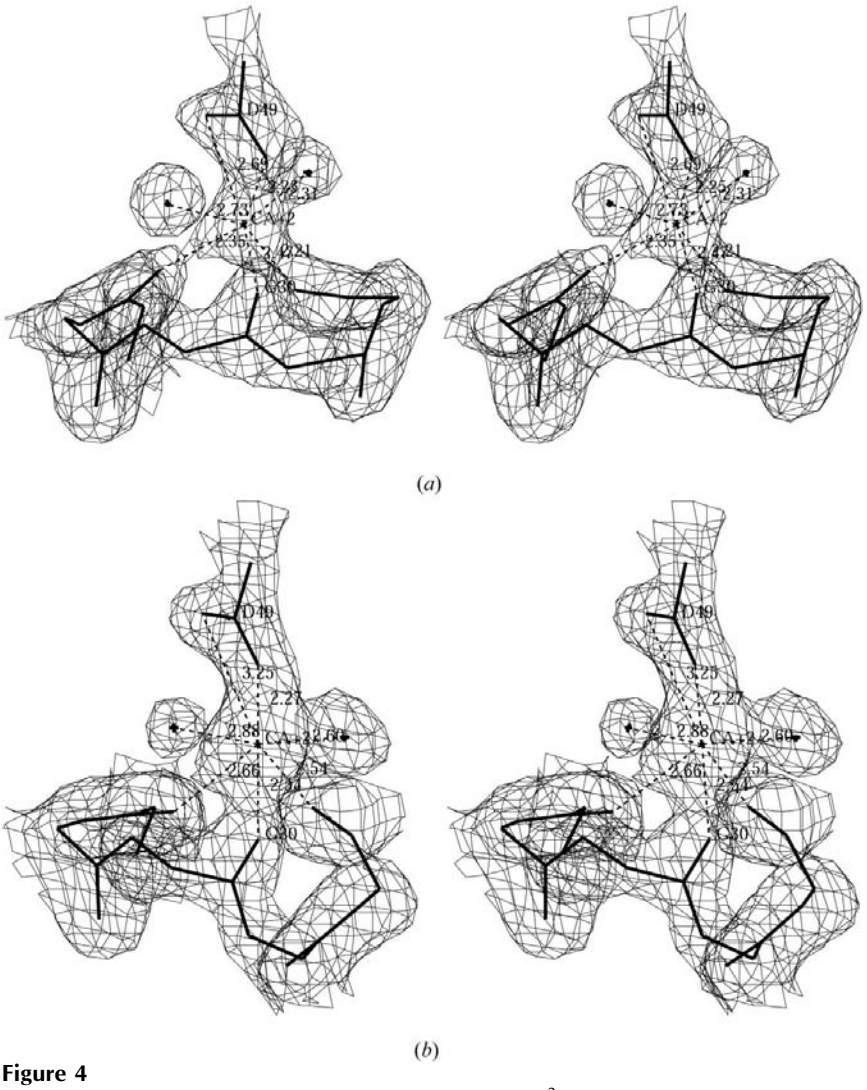

Figure 4
$2Fo - F_c$ electron-density map contoured at 1.0σ of the Ca^{2+}-binding loop in molecules *F* (*a*) and *B* (*b*).

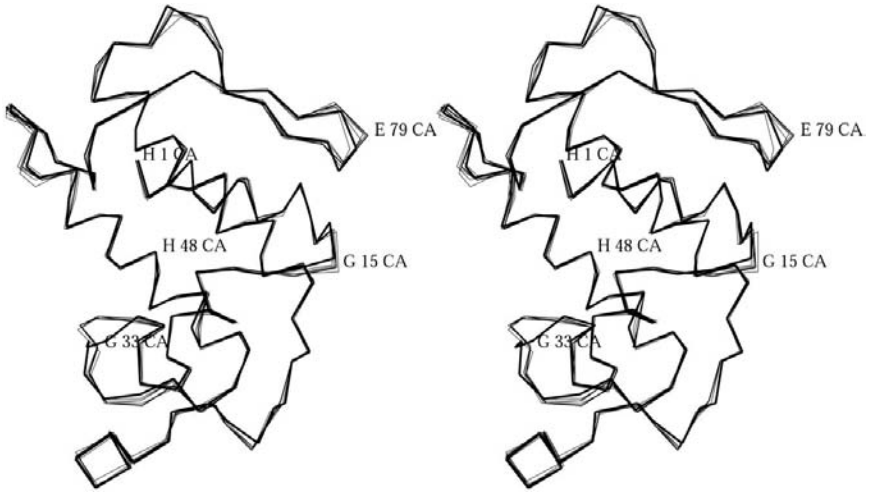

Figure 5
C^{α}-atom superposition of the six independent molecules. The bold line represents molecule *B*. Some conformational differences between these molecules are clearly shown.

OH $APLA_2$-II belongs to subgroup 1A, while OH $APLA_2$ belongs to subgroup 1B. It is unusual for one kind of snake venom to contain PLA_2s from two subgroups. The two PLA_2s have the same disulfide-bond pattern and a characteristic three-amino-acid 'elapid loop' composed of residues 54–56. The major sequence difference between them is the insertion of the pancreatic loop (62–66) in the latter. Figs. 6 and 7 show the superposition of the two structures and the deviation of their equivalent C^{α} atoms, respectively. A significant deviation occurs in segment 15–19. Another significant deviation occurs in segment 58–67 around and including the pancreatic loop, which only exists in OH $APLA_2$. With the removal of segments 15–19 and 58–67, the C^{α} r.m.s.d. value of the two structures is only 0.5 Å, indicating the remarkable similarity in overall three-dimensional structures between the two subgroups. The effect of the pancreatic loop on the molecular conformation is confined to a local region around the loop. It is improbable that the pancreatic loop transmits its conformational change to segment 15–19, as the latter is located on the opposite side of the molecule.

3.3. Catalytic activity and toxicity

Despite the high sequence homology, OH $APLA_2$ and OH $APLA_2$-II have obvious differences in their enzymatic activity. OH $APLA_2$-II is four times more active than OH $APLA_2$ (Wang, 2001). Comparing OH $APLA_2$-II with OH $APLA_2$ showed that they are extremely similar in the active site responsible for catalytic activity and the hydrophobic channel responsible for substrate binding, but that there is a distinct difference in the interface-recognition site (IRS). In PLA_2s, the IRS is responsible for efficient binding of the enzyme to the aggregated phospholipid–water interface. The IRS of OH $APLA_2$-II shows a plane-like structure, while the insertion of the pancreatic loop (residues 62–66) forms a protuberance on the IRS plane of OH $APLA_2$ (Fig. 6), resulting in an unfavorable binding to substrates in the aggregate state.

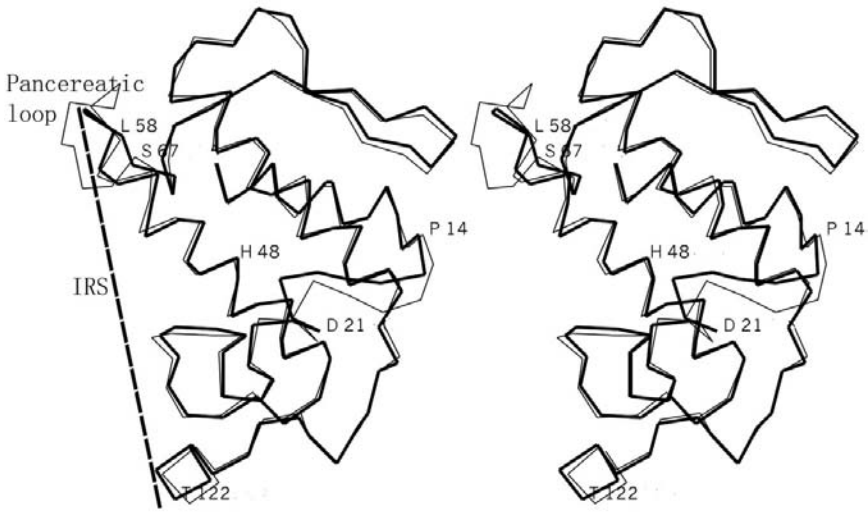

Figure 6
C^{α}-atom superposition of OH $APLA_2$-II and OH $APLA_2$, showing the overall structure (thick lines represent OH $APLA_2$-II).

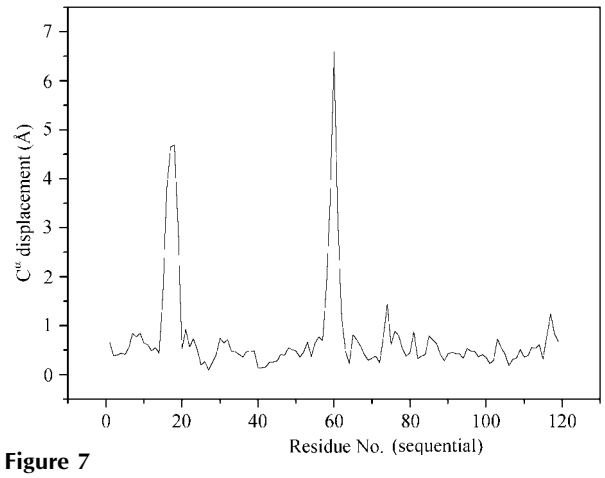

Figure 7
Distances between C^{α} pairs of OH $APLA_2$-II and OH $APLA_2$ along the polypeptide chain. The pancreatic loop is not included.

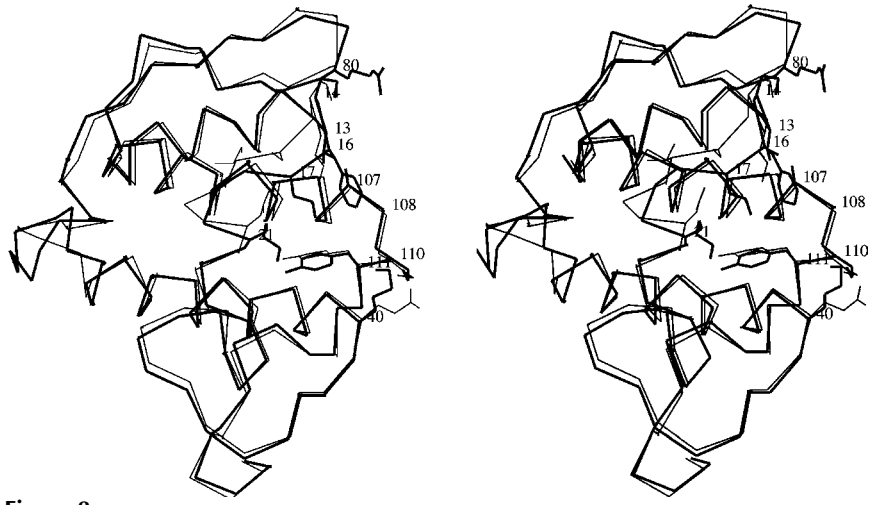

Figure 8
The comparison of a surface region surrounded by residues 21, 40 and 80 (thick lines represent OH $APLA_2$) using superposition matrix of C^{α} atoms. The residue numbers and side chains are shown. The significant conformational changes for segment 13–19 in this region can be discerned.

In addition, the pancreatic loop in OH $APLA_2$ is rich in hydrophilic residues (SSIMD), with the IRS being less hydrophobic compared with that of OH $APLA_2$–II without the loop. This crystallographic study supports the viewpoint that the planarity and hydrophobicity of the IRS in OH $APLA_2$-II results in a higher enzyme activity for aggregated substrates (Zhang *et al.*, 2002; Thunnissen *et al.*, 1990).

OH $APLA_2$ causes myotoxicity and cardiotoxicity in laboratory animals, but almost no myotoxicity and cardiotoxicity were observed on injection of OH $APLA_2$-II. The LD_{50} is 6.6 mg kg^{-1} for OH $APLA_2$ in mice, while the corresponding value is greater than 20 mg kg^{-1} for OH $APLA_2$-II. Structural comparison shows that except for the segment around and including the pancreatic loop discussed above, the only significant conformational difference between the two king cobra PLA_2s is located at segment 13–19, which might implicate this as the potential toxin site in OH $APLA_2$. To date, only a few snake-venom PLA_2s with cardiotoxic activity have been reported and structure–function studies of PLA_2-type cardiotoxins are even more rare. However, studies of non-PLA_2-type cardiotoxins (known as the three-finger family toxins) and PLA_2-type myotoxins have received wide attention. Both have indicated the importance of basic and hydrophobic residues in exerting myotoxic and cardiotoxic activities (Kumar *et al.*, 2000; Gutierrez & Lomonte, 1995). For OH $APLA_2$, although the overall charge is negative, some basic residues may be concentrated on a face of the molecule and provide a toxic site. Sequence comparison of toxic OH $APLA_2$ and low-toxicity OH $APLA_2$-II showed that four basic residues (Lys21, Lys40, Lys57 and Arg80) in OH $APLA_2$ were replaced by acidic or neutral residues (Asp21, Glu40, Gln57 and Gly80) in OH $APLA_2$-II. In the three-dimensional structure of OH $APLA_2$, the basic residues Lys21, Lys40 and Arg80 flank a surface region consisting essentially of hydrophobic residues involved in segments 13–19 and 107–111 (*i.e.* Val13, Pro14, Phe16, Leu17, Ala107, Ala108, Pro110 and Tyr111; Fig. 8). This region is distinctive and might be a potential toxicity site. Similar discussion has been mentioned by Zhang *et al.* (2002). The significant conformational changes observed for segment 13–19 in this region in comparison of the two king cobra PLA_2s support this viewpoint. Site-directed mutagensis studies are required to understand the structure–toxicity relationship of king cobra PLA_2 in depth.

This work was supported by National Natural Science Foundation of China (No. 3 9970174) and the Science Fund of the Chinese Academy of Sciences. We thank Dr Tao Jiang for most helpful discussions and Professor Zihe Rao and members of his group at Tsinghua University for their help during data collection and processing.

References

Arni, R. K. & Ward, R. J. (1996). *Toxicon*, **34**, 827–841.
Breyer, W. A., Kingston, R. L., Anderson, B. F. & Baker, E. N. (1999). *Acta Cryst.* D**55**, 129–138.
Brünger, A. T. (1992). *Nature (London)*, **355**, 472–475.
Brünger, A. T., Adams, P. D., Clore, G. M., DeLano, W. L., Gros, P., Grosse-Kunstleve, R. W., Jiang, J. S., Kuszewski, J., Nilges, M., Pannu, N. S., Read, R. J., Rice, L. M., Simonson, T. & Warren, G. L. (1998). *Acta Cryst.* D**54**, 905–921.
Chandra, N., Acharya, K. R. & Moody, P. C. E. (1999). *Acta Cryst.* D**55**, 1750–1758.
Chiou, J. Y., Chang, L. S., Chen, L. N. & Chang, C. C. (1995). *J. Protein Chem.* **14**, 451–456.
Davidson, F. F. & Dennis, E. A. (1990). *J. Mol. Evol.* **31**, 228–238.
Dijkstra, B. W., Drenth, J. & Kalk, K. H. (1981). *Nature (London)*, **289**, 604–606.
Gomis-Rüth, F. X., Fita, I., Kiefersauer, R., Huber, R., Aviles, F. X. & Navaza, J. (1995). *Acta Cryst.* D**51**, 819–823.
Gu, L., Zhang, H., Song, S., Zhou, Y. & Lin, Z. (2002). *Acta Cryst.* D**58**, 104–110.
Gutierrez, J. M. & Lomonte, B. (1995). *Toxicon*, **33**, 1405–1424.
Haas, G. H. de, Bonsen, P. P. M., Pieteson, W. A. & van Deenen, L. L. M. (1971). *Biochim. Biophys. Acta*, **239**, 252–266.
Huang, M. Z., Gopalakrishnakone, P., Chung, M. C. & Kini, R. M. (1997). *Arch. Biochem. Biophys.* **338**, 150–156.
Jones, T. A. (1978). *J. Appl. Cryst.* **11**, 268–272.
Kini, R. M. (1997). *Venom Phospholipase A_2 Enzymes: Structure, Function and Mechanism*, edited by R. M. Kini, pp. 1–28. New York: Wiley.
Kraulis, P. J. (1991). *J. Appl. Cryst.* **24**, 946–950.
Kumar, T. K. S., Sivaraman, T. & Yu, C. (2000). *Natural and Synthetic Toxins: Biological Implication*, edited by A.T. Tu & W. Gaffield, pp. 222–248. Oxford University Press.
Laskowski, R., MacArthur, M., Moss, D. & Thornton, J. (1993). *J. Appl. Cryst.* **26**, 283–290.
Merritt, E. A. & Bacon, D. J. (1997), *Methods Enzymol.* **277**, 505–524.
Otwinowski, Z. & Minor, W. (1997). *Methods Enzymol.* **276**, 307–326.
Ramachandran, G. N. & Sasisekharan, V. (1968). *Adv. Protein Chem.* **23**, 283–438.
Ramadan, M. A. M., Shrive, A. K., Holden, D., Myles, D. A. A., Volanakis, J. E., Delucas, L. J. & Greenhough, T. J. (2002). *Acta Cryst.* D**58**, 992–1001.
Redinbo, M. R. & Yeates, T. O. (1993). *Acta Cryst.* D**49**, 375–380.
Scott, D. L., White, S. P., Otwinowski, Z., Yuan, W., Gelb, M. H. & Sigler, P. B. (1990). *Science*, **250**, 1541–1546.
Tan, N. H. & Saifuddin, M. N. (1990). *Toxicon*, **28**, 385–392.
Thunnissen, M. M. G. M., Kalk, K. H., Drenth, J. & Dijkstra, B. W. (1990). *J. Mol. Biol.* **216**, 425–439.
Vagin, A. & Teplyakov, A. (1997). *J. Appl. Cryst.* **30**, 1022–1035.
Verheij, H. M., Volwerk, J. J., Jansen, E. H. J. M., Puyk, W. C., Dijkstra, B. W., Drenth, J. & de Haas, G. H. (1980). *Biochemistry*, **19**, 743–750.
Wang, Q. Y. (2001). MSc thesis, Guangxi Medical University, People's Republic of China.
Wang, Q. Y., Shu, Y. Y., Zhuang, M. X. & Lin, Z. J. (2001). *Acta Biochim. Biophys. Sin.* **33**, 340–344.
Wang, X. Q., Yang, J., Gui, L. L., Lin, Z. J., Chen, Y. C. & Zhou, Y. C. (1996). *J. Mol. Biol.* **255**, 669–676.
Wang, Z. Q., Zhuang, M. X., Shu, Y. Y., Zhang, H. L, Song, S. Y. & Lin, Z. J. (2001). *Acta Cryst.* D**57**, 709–710.
Wilson, A. J. C. (1949). *Acta Cryst.* **2**, 318–321.
Xu, S., Gu, L., Wang, Q., Shu, Y. & Lin, Z. (2002). *Acta Cryst.* D**58**, 1836–1837.
Yeates, T. O. (1997). *Methods Enzymol.* **276**, 344–358.
Zhang, H. L., Xu, S. J., Wang, Q. Y., Song, S. Y., Shu, Y. Y. & Lin, Z. J. (2002). *J. Struct. Biol.* **138**, 207–215.